

Mechanisms driving stratification in Delaware Bay estuary

María Aristizábal · Robert Chant

Received: 13 April 2013 / Accepted: 12 September 2014 / Published online: 2 October 2014
© Springer-Verlag Berlin Heidelberg 2014

Abstract An observational study in the middle reach of Delaware Bay shows that vertical stratification is often enhanced during flood tide relative to ebb tide, contrary to the tidal variability predicted by the tidal straining mechanism. This tidal period variability was more pronounced during times of high river discharge when the tidally mean stratification was higher. This tidal variability in stratification is caused by two reinforcing processes. In the along-channel direction, the upstream advection of a salinity front at mid-depth causes an increase of the vertical stratification during the flood tide and a decrease during the ebb tide. In the cross-channel direction, the tilting of isohalines during the ebb reduces vertical stratification, and the subsequent readjustment of the salinity field during the flood enhances the water column stability. A diagnosis of the cross-channel momentum balance reveals that the lateral flows are driven by the interplay of Coriolis forcing and the cross-channel pressure gradient. During the flood tide, these two forces mostly reinforce each other, while the opposite occurs during the ebb tide. This sets up a lateral circulation that is clockwise (looking landward) during the first half of the flood and then reverses and remains counterclockwise during most of the ebb tide. Past maximum ebb, the cross-channel baroclinic term, overcomes Coriolis and reverses the lateral flows.

Keywords Stratification · Tidal straining · Delaware Bay

1 Introduction

The mechanisms that control stratification in estuaries are central to estuarine dynamics and are important for biogeochemical processes, such as sediment transport, biological production, hypoxia, and carbon storage, among other processes. Stratification in these systems is driven by a competition between vertical mixing induced by wind and tides and the freshwater buoyancy input. These processes together establish the along-channel and vertical density gradients. At subtidal time scales, the estuarine exchange flow always promotes a stable water column, but the intensity of the stratification depends on the mixing strength controlled by, for example, the spring-neap cycle. On top of this background stratification, there is a tidal variability in stratification. Simpson et al. (1990) proposed the tidal straining mechanism to explain the periodic stratification observed in the region of freshwater influence (ROFI) of Liverpool Bay (Sharples and Simpson 1995; Rippeth et al. 2001). According to this mechanism, changes in stratification are caused by differential advection, due to the vertical shear of the tidal velocities acting on the horizontal density gradient.

Observations in the Rhine ROFI also showed large semidiurnal variations in stability under conditions of weak vertical mixing (Simpson and Souza 1995; Souza and Simpson 1995). These semidiurnal variations are caused by a cross-shore tidal straining, which interacts with the density gradient to induce or reduce stratification. This cross-shore tidal straining is driven by a two-step process: first, stratification causes a decoupling of the surface and bottom tidal ellipses (Souza and Simpson 1996), and second, the minor

Responsible Editor: Rockwell Geyer

This article is part of the Topical Collection on *Physics of Estuaries and Coastal Seas 2012*

M. Aristizábal (✉) · R. Chant
Rutgers University, 71 Dudley Road, New Brunswick,
NJ 08901, USA
e-mail: aristizabal@marine.rutgers.edu

axis component of the tidal ellipses drives the subsequent straining. This contrasts with the Liverpool ROFI, where the straining is caused by the main-axis component of the almost rectilinear tidal ellipse. Whether the main or minor axis of the tidal ellipses is the one that strains the density field depends on which component is aligned with the density gradient.

Semidiurnal changes in stratification have also been observed in a variety of estuaries (Jay and Smith 1990; Sharples et al. 1994; Nepf and Geyer 1996; Stacey et al. 1999; Chant and Stoner 2001; Cheng et al. 2009). In these systems where tidal flows are highly elongated, it is the shear in the along-channel tidal velocities that interact with the along-channel density gradient to produce the tidal variations in vertical stability. These variations are such that the water column is well mixed at the end of flood and reaches maximum stability at the end of ebb (Simpson et al. 1990). Nevertheless, there have been observational studies in a number of systems that have shown that this tidal variability in stratification is not always apparent. For example, observations in a channel in northern San Francisco Bay (Lacy et al. 2003) showed that vertical stratification can develop during spring flood tides. This is because during these periods, the lateral density gradient far exceeded the longitudinal density gradient, and stratification was caused by the lateral baroclinic forcing that surpassed turbulent mixing. More recently, Scully and Geyer (2012) also showed that in the upper Hudson, tidal variations in stratification are not consistent with the along-channel straining mechanism. They attributed this to a competition between the along-channel and cross-channel advection of vertical salinity gradients ($\partial s/\partial z$) and tidal asymmetries in vertical mixing. These processes are likely to be negligible during well-mixed conditions because as $(\partial s/\partial z)$ becomes small, both longitudinal advection of stratification and cross-channel density gradients are reduced. This implies that a periodic stratification that agrees with longitudinal tidal straining is more likely to manifest during well-mixed periods such as that found in Liverpool Bay (Simpson et al. 1990).

In a numerical simulation in Chesapeake Bay, Li and Li (2012) found that the lateral wind-driven flows can tilt or flatten the isohalines in the cross-channel direction, creating a lateral baroclinic pressure gradient that opposes or reinforces the lateral wind-driven Ekman transport. In addition, vertical stratification is reduced when the isohalines are vertically tilted, but is enhanced when the isohalines flatten. This wind-induced straining can compete with the along-channel straining mechanism.

In order to quantify the different processes that control stratification, Simpson and Hunter (1978) defined the potential energy anomaly ϕ as the total amount of work per unit volume required to completely mix the water column. The potential energy anomaly has been used as a

framework in a number of observational and numerical studies. Simpson and Hunter (1974), Simpson (1981), and Simpson and Bowers (1981) studied the behavior of fronts in the shelf seas around the UK, assuming surface heating as the only source of stratification and stirring due to winds and tidal stresses as the destabilizing source. Simpson et al. (1990) then expanded their analysis to estuaries by including the effects of horizontal density gradients induced by freshwater buoyancy inputs at the boundaries. Later, de Boer et al. (2008) derived a dynamic equation for ϕ that was suitable for the analysis of 3D models and applied it to an idealized simulation of the Rhine ROFI. They assumed a constant depth and zero surface and bottom density fluxes. Furthermore, Burchard and Hofmeister (2008) rigorously derived $\partial\phi/dt$ based on the dynamic equations for temperature and salinity, the continuity equation, and the nonlinear equation of state for seawater. All these studies demonstrated that the potential energy anomaly is an extremely useful tool to quantify the different mechanisms that control stratification in estuaries and coastal seas.

Our observations in Delaware Bay on the East Coast of the USA show substantial changes in stratification levels at tidal time scales, but this variability is opposed to the one predicted by the tidal straining mechanism. The aim of this work is to understand the physical mechanisms that mediate this tidal variability in stratification by using the potential energy anomaly approach and an analysis of the cross-channel momentum balance.

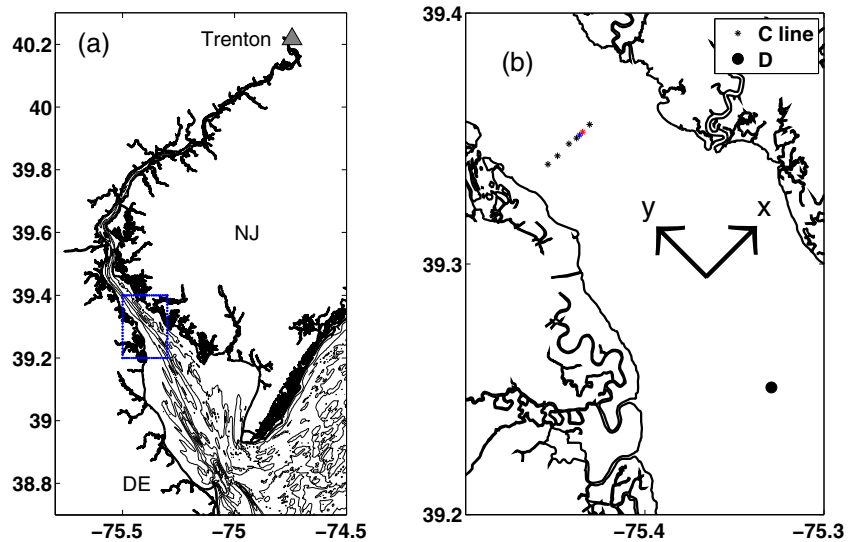
2 Study site

Delaware Bay is a coastal plain estuary located on the East Coast of the USA. Its main tributary is the Delaware River, which accounts for 50–60 % of the total freshwater input into the bay. The Schuylkill River and Christina River are the second and third rivers in importance and contribute 15 and 8 %, respectively (Wong 1994). Based on statistics from a 100-year record (USGS 2012), the mean annual Delaware River discharge at Trenton is 342 m³/s and averages ≈ 200 m³/s during the summer and fall but increases to ≈ 630 m³/s during the spring freshets, and it can exceed 5000 m³/s during extreme events.

The bathymetry of the system is characterized by shallow flanks and a deep main channel that has been dredged since the late nineteenth century. The bay's mean depth is 8 m with a maximum depth of 45 m. This system's geometry is simple (Fig. 1) with a mouth that is 18 km wide and a maximum width of 40 km at 17 km from the entrance of the bay. Beyond this point, the system narrows, resembling a funnel shape.

In the literature, Delaware Bay has been classified as a weakly stratified estuary (Beardsley and Boicourt 1981;

Fig. 1 **a** Delaware Bay map with bathymetry contours. The location of Trenton, the head of the tides, is shown as a *gray triangle*. **b** Detail of the area in the *blue rectangle* in **a** showing the location of the mooring array



Garvine et al. 1992), but from our observations, we see that this system can have a bottom-to-surface salinity difference exceeding 10 during periods of high river discharge, but is almost vertically well mixed for periods of low river discharge particularly during spring tide conditions. The location of the head of the salt has been monitored by USGS for several decades and is located between 90 and 140 km from the entrance of the bay with a mean along-channel salinity gradient of 0.34 km^{-1} (Garvine et al. 1992).

Lateral variations of salinity are quite significant in this system and play an important role in its dynamics, as suggested by Wong (1994) and in the analysis presented here. From observations, we obtained a cross-channel salinity gradient, between the main channel and the Delaware flank, that fluctuates from about $1.0(1 / \text{km})$ at the end of ebb tide to close to 0 or small negative values at the end of flood tide. The flanks tend to be fresher than the main channel, with the Delaware side being the freshest due to the Coriolis acceleration trapping the outflowing water to the bay’s southern shore.

3 Field program

From April 8 to June 27, 2011 we deployed a mooring array in the middle reach of Delaware Bay, consisting of a six-element cross-channel array (C-line) and a single mooring (D mooring) located at 68 and 54 km, respectively, from the entrance of the bay (Fig. 1). This paper focuses on three of the moorings along the C-line: the C2 mooring with a bottom mounted with 1200-kHz Acoustic Doppler Current Profiler (ADCP) and a surface, mid-depth, and bottom CT sensor; the C5 mooring with a bottom mounted with 1200-kHz ADCP; and a string of four CT sensors that spanned the water column deployed from a Coast Guard

Navigational Buoy (CG) (Fig. 2). These two moorings had the most complete records because the other time series were shortened due to fouling or other technical issues. Moreover, they were well positioned to characterize the lateral dynamics. The D mooring had a bottom mounted with 600-kHz ADCP and a surface and bottom CT sensor. The ADCPs were programmed to acquire data for a period of 2 min at a rate of 1 Hz, every 10 min. These measurements were averaged for a total of six ensembles per hour. The vertical resolution was 0.5 m for the D mooring and 0.25 m for the C2 and C5 moorings. The CT sensors acquired data every 10 min.

Additionally, two cross-channel tidal surveys (corresponding to periods of neap and spring tide) were performed on the same location of the C-line on April 13 and 19, 2011. The surveys consisted of hourly transects with a

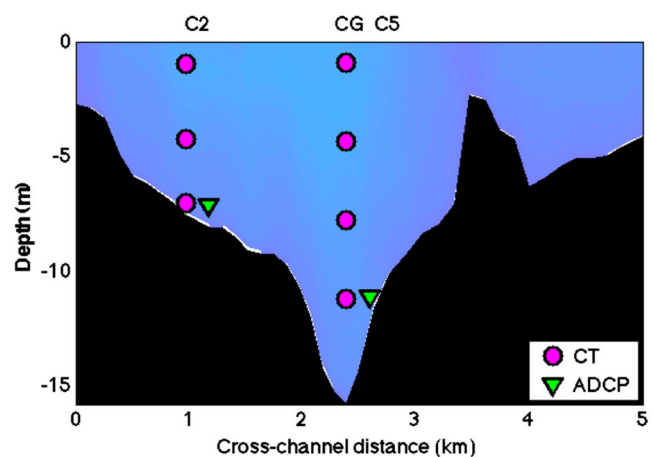


Fig. 2 Cross section of Delaware Bay at the C-line (69 km from the entrance of the bay) showing the different instruments deployed at this location. In this figure, the right flank is on the New Jersey side and the left flank on the Delaware side

downward-looking 1200-kHz ADCP over a period of 13 h. Other instruments included CT and OBS sensors. These instruments were mounted in a cage that was manually lowered and provided measurements from the surface to within 2 m from the bottom with a horizontal resolution of about 130 m. We only present data from the April 13 survey because on April 19, the water column became nearly fresh at the end of the ebb tide.

4 Methods

Principal component analysis was performed on the depth-averaged velocities from the C5 mooring, and the velocities were projected onto the along-channel and cross-channel directions accordingly. The horizontal coordinate system is shown in Fig. 1b, with the y - and x -axes denoting the along-channel and cross-channel directions, respectively. In our convention, positive values represent the landward direction on the y -axis and the northeast direction (towards the New Jersey flank) on the x -axis. We defined a vertical coordinate system that is positive downward, with H denoting the bottom of the water column and 0 the surface. The velocities measured at C5 covered approximately 73 % of the water column from 0.87 m above bottom to 2.9 m below the surface due to sidelobe interference with the surface. These velocity profiles were then extrapolated to the surface using a parabolic profile and to the bottom with a logarithmic profile with a bottom roughness of $z_0 = 0.04$ m above the bed. These full-water column velocity profiles were then converted into a terrain-following coordinate system with 40 evenly spaced vertical levels. Additionally, a 3-h low-pass filter was applied to all velocity and salinity data to eliminate high-frequency variations when calculating the different terms in the salinity and momentum equations.

4.1 Potential energy anomaly and salinity equation

The potential energy anomaly and its time rate of change were calculated for the CG mooring following (Simpson et al. 1990):

$$\phi = \frac{g\beta}{H} \int_0^H (\bar{s} - s)zdz \quad (1)$$

$$\frac{\partial \phi}{\partial t} = \frac{g\beta}{H} \int_0^H \left(\frac{\partial \bar{s}}{\partial t} - \frac{\partial s}{\partial t} \right) z dz \quad (2)$$

where g is the gravitational acceleration, β is the haline expansion coefficient, s is salinity at different depths, and $\bar{s} = \frac{1}{H} \int_0^H s dz$ is the depth-averaged salinity. H is the bottom of the water column and 0 is the surface. In Eq. 2, we

have neglected the periodic changes of ϕ due to tidal variations in H because the inclusion of $\partial H/\partial t$ did not have a substantial effect on the results. In order to perform the integrations in Eqs. 1 and 2, we defined a vertical grid where the CT sensors are located approximately in the middle of each grid cell at a distance z from the surface. Defined this way, $\phi = 0$ represents a homogenous water column and a negative ϕ a stratified water column. The more negative ϕ is, the stronger is the stratification; thus, a negative $\partial \phi/\partial t$ means that stratification is being enhanced and a positive $\partial \phi/\partial t$ means that stratification is being reduced.

Meanwhile, the salinity equation can be written as follows:

$$\frac{\partial s}{\partial t} = -v \frac{\partial s}{\partial y} - u \frac{\partial s}{\partial x} - w \frac{\partial s}{\partial z} + \frac{\partial}{\partial z} \left(\frac{K_s \partial s}{\partial z} \right) \quad (3)$$

where v , u , and w are the along-channel, cross-channel, and vertical velocity, respectively. $\partial s/\partial y$, $\partial s/\partial x$, and $\partial s/\partial z$ are the along-channel, cross-channel, and vertical salinity gradients. $\frac{\partial}{\partial z} (K_s \frac{\partial s}{\partial z})$ is the time rate of change of salinity due to vertical mixing, and K_s is the vertical eddy diffusivity of salt. The along-channel salinity gradient was calculated using the salinity at the surface and bottom of the D and CG mooring. The cross-channel salinity gradient was calculated using salinity at three different depths between the CG and C2 mooring.

Additionally, the along-channel velocity can be divided in three different components (MacCready 2011):

$$v_0(t) = \frac{1}{\langle \int dz \rangle} \left(\int v(z, t) dz \right) \quad (4)$$

$$v_e(z, t) = \frac{\langle v dz \rangle}{\langle dz \rangle} - v_0 \quad (5)$$

$$v_t(z, t) = v - v_e - v_0 \quad (6)$$

where the brackets $\langle \rangle$ represent a low-pass filter to remove oscillations at tidal time scales. We used a 32-h Lanczos low-pass filter with a 70-h half window. Under this decomposition, v_0 represents the river discharge velocity but may include other contributions such as meteorologically forced flows. v_e is the estuarine exchange flow, and v_t is the tidal component of velocity. Then the depth-dependent and the depth-averaged salt equations can be expressed as follows:

$$\frac{\partial s}{\partial t} = -(v_0 + v_e + v_t) \frac{\partial s}{\partial y} - u \frac{\partial s}{\partial x} - w \frac{\partial s}{\partial z} + \frac{\partial}{\partial z} \left(\frac{K_s \partial s}{\partial z} \right) \quad (7)$$

$$\frac{\partial \bar{s}}{\partial t} = -(v_0 + \bar{v}_t) \frac{\partial \bar{s}}{\partial y} - \bar{v} \left(\frac{\partial \bar{s}}{\partial y} \right)' - u \frac{\partial \bar{s}}{\partial x} - w \frac{\partial \bar{s}}{\partial z} + \frac{\partial}{\partial z} \left(\frac{K_s \partial s}{\partial z} \right) \quad (8)$$

where the overbar represents a depth average: $\bar{(\)} = \frac{1}{H} \int_0^H (\) dz$. In Eq. 8, we decomposed the along-channel salinity gradient as the sum of a depth-averaged and depth-varying component: $\partial s/\partial y = \bar{\partial s/\partial y} + (\partial s/\partial y)'$. We have also used the fact that the depth average of v_e is zero.

Then Eq. 2 can be expressed as follows:

$$\begin{aligned} \frac{\partial \phi}{\partial t} = & \frac{g\beta}{H} \int_0^H \left(\underbrace{v_e \frac{\partial s}{\partial y}}_{\text{exchange}} + \underbrace{(-\bar{v}_t + v_t) \frac{\partial s}{\partial y}}_{\text{along-tidal}} + \underbrace{\left(-u \frac{\partial s}{\partial x} + u \frac{\partial s}{\partial x}\right)}_{\text{cross-tidal}} \right) \\ & + \underbrace{\left(-v \left(\frac{\partial s}{\partial y}\right)' + v \left(\frac{\partial s}{\partial y}\right)'\right)}_{\text{along-adv. strat.}} \\ & + \underbrace{\left(-w \frac{\partial s}{\partial z} + w \frac{\partial s}{\partial z}\right) + \frac{\partial}{\partial z} \left(\frac{K_s \partial s}{\partial z}\right) - \frac{\partial}{\partial z} \left(\frac{K_s \partial s}{\partial z}\right)}_{\text{residual}} \right) z dz. \end{aligned} \quad (9)$$

The “exchange” term expresses the contribution of the estuarine circulation to stratification. The “along-tidal” term represents the contribution of the shear in the along-channel tidal velocity, which corresponds to the tidal straining mechanism introduced by Simpson et al. (1990). Likewise, the “cross-tidal” term can be interpreted as the effect that the shear in the cross-channel flows have on vertical stability. The “along-adv. strat.” represents the along-channel advection of stratification due to vertical variations of the along-channel salinity gradient. The “residual” term is the sum of the contributions from vertical advection and mixing and can not be calculated directly with the available data.

When calculating the different terms in Eqs. 7, 8, and 9, $\frac{\partial s}{\partial y}$ was low-passed, but the tidal variability of $\frac{\partial s}{\partial x}$ was retained because it changes signs during the tidal cycle and this affects the time rate of change of the potential energy anomaly at tidal time scales. The tidal variability of $\frac{\partial s'}{\partial y}$ was also retained, as this term quantifies how stratification is advected in the along-channel direction at tidal time scales.

4.2 Cross-channel momentum equation

The cross-channel momentum equation can be expressed as follows:

$$\frac{\partial u}{\partial t} = -g \frac{\partial \eta}{\partial x} - \frac{g}{\rho_0} \frac{\partial \rho}{\partial x} z + f v + \frac{1}{\rho_0} \frac{\partial \tau_u}{\partial z} \quad (10)$$

where u and v are the cross- and along-channel velocity, respectively; g is the gravitational acceleration; η is the sea surface elevation; ρ is the density of sea water; f is the Coriolis frequency; and τ_u is the stress in the cross-channel direction. In Eq. 10, the advection terms have been neglected because of the following scaling arguments. The lateral and vertical advection terms can be scaled as u^2/W and wu/H , where W is the width of the channel, H is the depth of the water column, and w is vertical velocity. If we take a typical values for this quantities: $u \sim 10^{-1}$ m/s, $w \sim 10^{-3}$ m/s, $H \sim 10$ m, and $W \sim 10^4$ m we obtain that

both terms are of the order of 10^{-6} and 10^{-5} , respectively, which is at least 1 order of magnitude less than the leading terms in Eq. 10. The along-channel advection term can be scaled as vu/L , where L represents an along-channel distance where u have a significant change in magnitude. An enhancement of the lateral flows can happen around bends (Chant 2002), and since the mooring array is located in a straight section of the channel, we assume that this term should be relatively small as well. The first two terms on the right side of Eq. 10 are the barotropic and baroclinic contributions of the cross-channel pressure gradient, fv is the Coriolis acceleration, and the last term is the vertical stress divergence. We do not have an accurate estimate for the barotropic pressure gradient, but this term can be eliminated by subtracting the depth-averaged cross-channel momentum equation from the depth-dependent equation. This yields

$$\begin{aligned} \underbrace{\frac{\partial(u - \bar{u})}{\partial t}}_{\text{accel}} = & -\frac{g}{\rho_0} \underbrace{\left(\frac{\partial \rho}{\partial x} z - \frac{\partial \rho}{\partial x} \bar{z}\right)}_{\text{prsgrd}} + \underbrace{f(v - \bar{v})}_{\text{cor}} \\ & + \underbrace{\frac{1}{\rho_0} \left(\frac{\partial \tau_u}{\partial z} - \frac{\tau_0 - \tau_H}{H}\right)}_{\text{vvisc}}. \end{aligned} \quad (11)$$

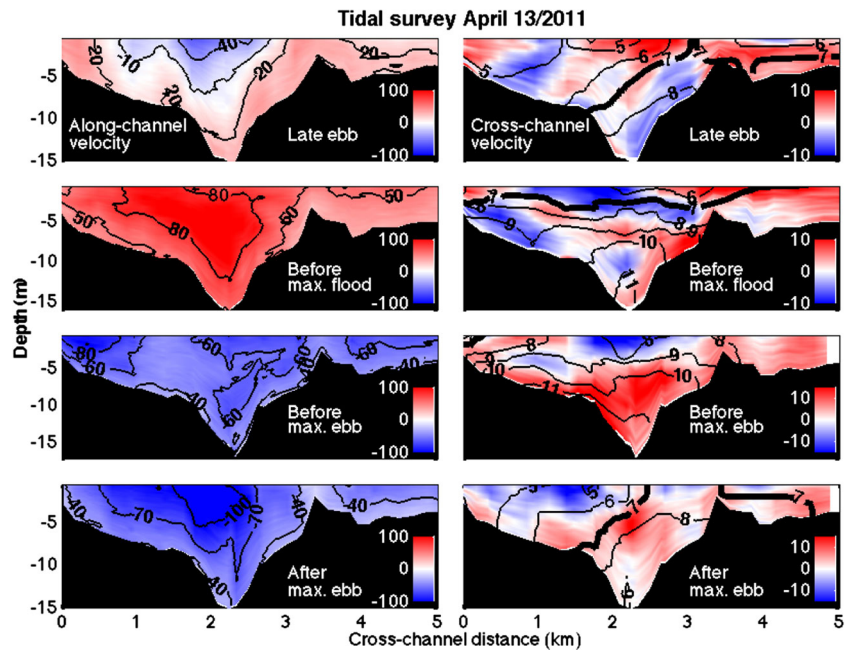
This equation represents the tendency to drive cross-channel shear by the different forces. For example, the Coriolis acceleration term, “cor,” has opposite signs at the surface and bottom because this term is proportional to the velocity profile v minus its depth average \bar{v} . Therefore, this term tends to drive an one cell circulation. The baroclinic pressure gradient term (“prsgrd”) is proportional to $(z - \bar{z})$, assuming that $\frac{\partial \rho}{\partial x}$ is depth independent. In this case, this term is not zero at the surface but equal to the depth-averaged baroclinic pressure gradient: $\frac{g}{\rho_0} \frac{\partial \rho}{\partial x} \bar{z}$, and at depth it has an opposite sign than at the surface: $\frac{g}{\rho_0} \frac{\partial \rho}{\partial x} (\bar{z} - H)$. The vertical viscosity term “vvisc” is the deviation of the vertical gradient of the interfacial stress from its depth average $\frac{\tau_0 - \tau_H}{H}$ where τ_0 is the wind surface stress and τ_H is the bottom stress.

5 Results

5.1 Cross-channel tidal surveys

On April 13, 2011, at the beginning of the deployment period, we performed the first cross-channel tidal survey during neap tide and a river discharge at Trenton of $640 \text{ m}^3/\text{s}$. The tidal cycle survey provided a detailed view of the cross-channel structure of velocity and salinity and its variability over a tidal cycle. The first transect shown in Fig. 3 (upper panels) corresponds to the end of the ebb tide, and the bottom to surface salinity difference is about 3 in the

Fig. 3 Cross-sectional transects from the tidal survey on April 13, 2011, for different tidal phases. The oceanward direction points out of the page. The along-channel velocity panels show contours of along-channel velocity with the color scale in centimeters per second and positive values indicating landward direction. The cross-channel velocity panels show contours of salinity over imposed on the cross-channel velocity in centimeters per second and positive values towards the right flank (New Jersey side)



middle of the channel, with the isohalines slightly tilted. Once the flood tide develops (Fig. 3, second row), the isohalines become horizontal and the stratification increases to a maximum value of 5. During the first half of the ebb tide (Fig. 3, third row), the vertical stratification starts to drop and reaches its minimum value after maximum ebb (Fig. 3, bottom panels) with a value of 2. This tidal variability in stratification is contrary to the variability expected from tidal straining mechanism introduced by Simpson et al. (1990). The cross-channel flows had a significant spatial and temporal variability. The most important features of

these flows in the middle of the channel are a clockwise circulation during the late ebb/early flood, two counter-clockwise cells around maximum flood, and a clear counterclockwise cell during the rest of ebb tide.

A similar tidal variability in stratification was also captured by the moored data. In what follows, we will present further evidence for the tidal variability in stratification that we just described, and we will try to understand more quantitatively how the cross-channel flows bring about this variability and what are the underlying dynamics that drive these cross-channel flows.

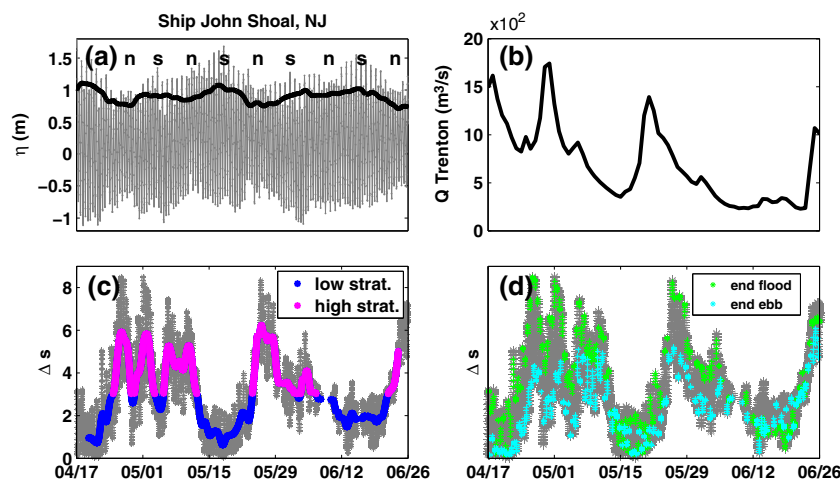


Fig. 4 **a** Time series of mean sea level from the NOAA station at Ship John Shoal. The *black thick line* shows the mean sea level amplitude. The figure also shows periods of neap and spring tide during the time of the deployment. **b** Delaware River discharge measured at Trenton (New Jersey). **c** Bottom to surface salinity difference Δs from the CG mooring (*gray line*) for the time of the deployment. The *color lines*

are the low-passed signal of Δs . This low-passed signal is classified in times of low stratification (*blue line*) and high stratification (*magenta line*) based on the mean of the low-passed Δs ($\langle \Delta s \rangle = 3.0$). **d** Δs from the NG mooring highlighting the Δs value for two tidal phases: end of flood (*green*) and end of ebb (*cyan*)

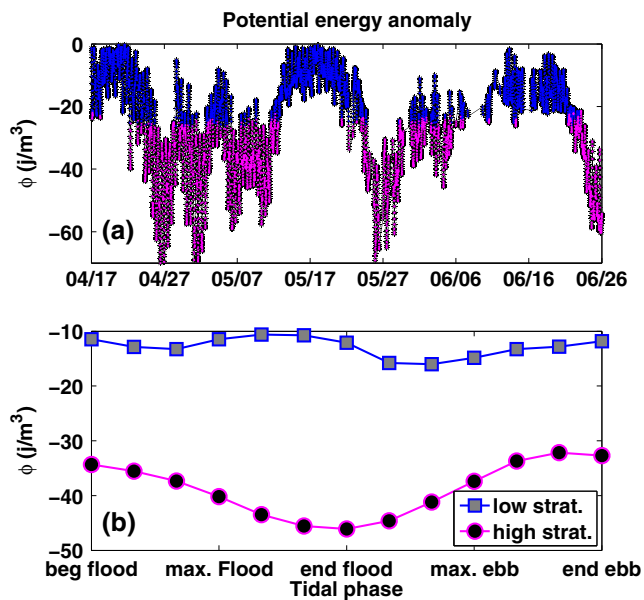


Fig. 5 **a** Time series of the potential energy anomaly from the CG mooring. The *magenta* and *blue* lines show times of high and low stratification, respectively, as defined in Fig. 5c, based on the mean of the low-passed Δs ($< \Delta s > = 3.0$). **b** Tidal phase average of the potential energy anomaly for times of high and low stratification

5.2 Stratification conditions

The bottom-to-surface salinity difference Δs from the CG mooring varied from a maximum of 8.5 to very close to zero (Fig. 4c). In this study, the periods of high stratification corresponded to times of river discharge of around 1500 m³/s and neap tides, while periods of low stratification coincided with times of the lowest river discharge of the deployment,

~ 400 m³/s, and spring tides. The first week of May is an exception to this stratification pattern: it is well stratified in spite of spring tide conditions, but the river discharge is the highest of the observation period. For this reason, periods of low (high) stratification were defined as times when the low-pass filter of Δs was less (greater) than the average Δs for the whole study, rather than using tidal amplitude (i.e., spring/neap (Fig. 4a)) as a proxy.

The values of Δs in the middle of the channel corresponding to the end of flood and the end of ebb are shown in Fig. 4d. For periods of high stratification, Δs is the largest at the end of flood tide and is significantly reduced at the end of ebb tide. On the other hand, during periods of low stratification, Δs is either similar for these two tidal phases or larger at the end of the ebb tide. The tidal phase average of ϕ (Fig. 5), representing a bulk measure of stratification, also reveals that late flood stratification is enhanced during periods of high river discharge and that is larger on flood relative to ebb.

5.3 Along and cross-channel salinity gradient

During the time of the deployment, the river discharge at Trenton had a maximum value of approximately 1744 m³/s and a minimum of 228 m³/s (Fig. 4b). The along-channel salinity gradient between the CG and D mooring, $\partial s/\partial y$, fluctuated around -0.45 (1/km) (Fig. 6a), and its low-pass signal was highly correlated with river discharge (Fig. 6b) with a maximum correlation of 0.76 for a lag of 3 days.

On the other hand, the cross-channel salinity gradient ($\partial s/\partial x$) between the CG and C2 mooring at 8-m depth fluctuates between positive and negative values, with

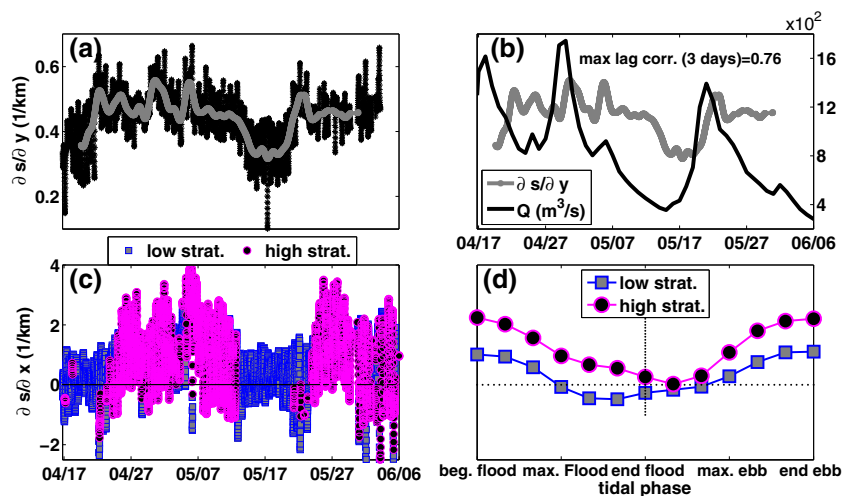


Fig. 6 **a** Time series of the depth-averaged along-channel salinity gradient (*black* line) and its low-pass signal (*gray* line). **b** Delaware River discharge at Trenton along with the low-pass of the along-channel salinity gradient. They have a maximum correlation of 0.76 for a time lag of 3 days. **c** Time series of the cross-channel salinity gradient at

8-m depth, between the C2 and CG moorings. The *magenta* and *blue* lines show times of high and low stratification, respectively. **d** Tidal phase average of the cross-channel salinity gradient in **c** for times of high and low stratification

positive values indicating a main channel that is saltier than the Delaware flank. The amplitude of $\partial s/\partial x$ is about five times larger than the average value of $\partial s/\partial y$ (Fig. 6c) with greater positive values during periods of high stratification. This positive correlation indicates that $\partial s/\partial x$ also responds to changes in river discharge, since high stratification periods corresponded to high river discharge conditions as discussed in Section 5.2. When a tidal phase average is performed on $\partial s/\partial x$ (Fig. 6d), we see that the positive values occur from maximum ebb through slack water and into the flood, as isohalines become vertical and the main channel becomes saltier than the left flank (Delaware side) during this phase of the tide. The cross-channel gradient is near zero or weakly negative during the second half of the flood through the first half of the ebb as isohalines flatten. This tidal variability of $\partial s/\partial x$ plays an important role in the cross-channel dynamics as will be discussed later.

5.4 Salt balance

The time rate of change of salinity, the along-channel advection, and cross-channel advection terms were calculated directly from this data set by using the salinity data from the CG and D mooring and the velocity profiles from the C5 mooring.

The depth-averaged salt equation (Fig. 7a) shows that there is a close balance between $\frac{\partial \bar{s}}{\partial t}$ and $-\bar{v}_t \frac{\partial \bar{s}}{\partial y}$, meaning that in a depth-averaged sense, the time rate of change of salinity is caused primarily by the along-channel advection of the tidal flows. The term $-v_0 \frac{\partial s}{\partial y}$ is relatively small because v_0 is about 1 order of magnitude smaller than v_t . Additionally, $-\bar{u} \frac{\partial s}{\partial x}$ is also quite small because the depth-averaged cross-channel flow is close to zero in the middle of the main channel, consistent with a closed cell.

The depth-dependent salt equation shows that the cross-channel advective term is small at the surface and at depth (Fig. 7b, c). The terms $-v_e \frac{\partial s}{\partial y}$ and $v_0 \partial s/\partial y$ are negligible because v_0 and the subtidal velocity are 1 order of magnitude smaller than v_t . The sum of the along- and cross-channel advective terms does not equal the time rate of change of salinity, especially close to maximum ebb and flood tide. The discrepancy is certainly in part due to mixing, but other processes not resolved with the array also contribute. For example, at the surface, the mixing contribution to $\partial s/\partial t$ is always positive since saltier layers of water, lower in the water column, are being vertically mixed. Therefore, during the flood tide, mixing and along-channel advection are both positive and this should yield a total $\partial s/\partial t$ that is larger than $-v \partial s/\partial y$, which is not the case in Fig. 7a. In contrast, during the ebb tide, there is a large discrepancy with the magnitude of $\partial s/\partial t$ smaller than that of $-v \partial s/\partial y$, and this is consistent with mixing in that at the surface during the ebb, mixing competes with along-channel advection.

5.5 Time rate of change of the potential energy anomaly

$\partial \phi/\partial t$ (9) is expressed as different contributions to stratification: exchange, along-channel tidal, cross-channel tidal, along-channel advection of stratification, and residual. The last term is the sum of the vertical advection and mixing contributions.

The time series of the horizontal advection contributions to stratification (Fig. 8a) shows that the “along-tidal” and “along-adv. strat.” contributions are dominant and that the “exchange” and “cross-tidal” contributions are smaller but not insignificant. This contrasts with the relatively small contributions that the cross-channel and exchange advection have in the depth-dependent salinity equation. This

Fig. 7 Detail of the time series of the salt balance between March 10 and 12, 2011. **a** Depth-averaged salt equation (8). **b** Salt equation (7) at 1 m below the surface. **c** Salt equation (7) at 8 m below the surface

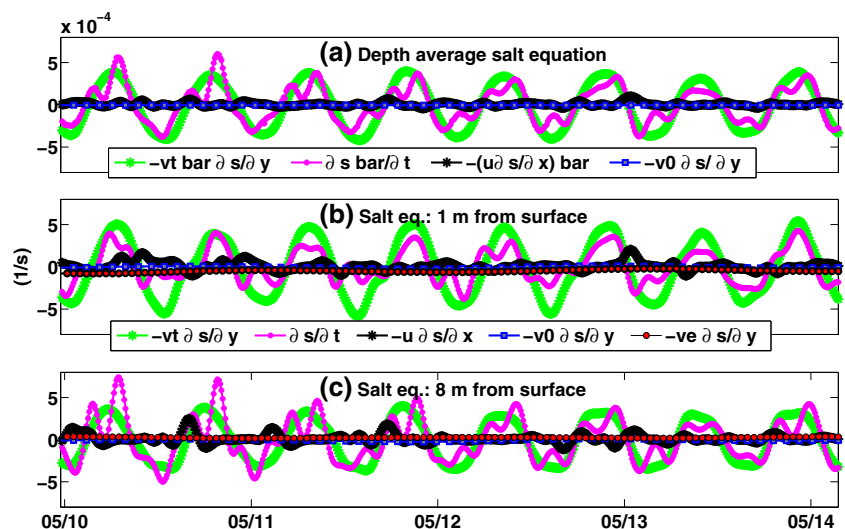
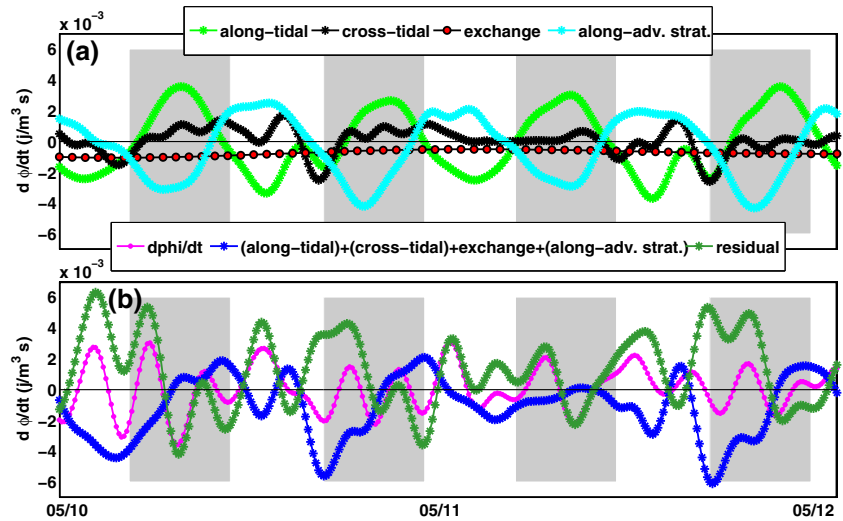


Fig. 8 Detail of the time series of the time rate of change of the potential energy anomaly as shown in Eq. 9 between March 10 and 12, 2011. **a** Four advective terms: “along-tidal,” “cross-tidal,” “exchange,” and “along-adv. strat.” **b** Total $\partial\phi/\partial t$, the sum of the four advective terms, and the residual, equal to $\partial\phi/\partial t$ - advective terms. The shaded areas represent periods of flood tide



emphasizes the importance of using a depth-integrated quantity as the potential energy anomaly. Figure 8b shows the time series of $\partial\phi/\partial t$, the sum of the four horizontal advection terms (“along-tidal”, “exchange”, “cross-tidal”, “along-adv. strat.”) and the residual. The sum of the horizontal advection terms does not balance $\partial\phi/\partial t$, and therefore the residual term is very significant. This suggests that mixing and vertical advection are also important.

A tidal phase average is performed on the different terms of Eq. 9, considering times of low and high stratification (Fig. 9). We noted that the along-tidal contribution has a de-stratifying effect during most of the flood (positive $\partial\phi/\partial t$) and a stratified effect during ebb tide (negative $\partial\phi/\partial t$), consistent with the tidal straining mechanism. The exchange component has always a stratifying action corresponding to a two-layer exchange flow, so it is enhanced during periods of high stratification. On the other hand, the cross-tidal component tends to stratify during the first half of the flood

and de-stratify at the end of the ebb for periods of both low and high stratification, having an opposite effect than the along-channel contribution, but its magnitude is not large enough to overcome the action of the along-channel straining. The contribution of along-adv. strat., which represents the along-channel advection of stratification due vertical variations of the along-channel salinity gradient, is as large as the along-tidal contribution. The “along-adv. strat.” has the opposite effect than the along-channel straining: it stratifies the water column during the flood and de-stratifies it during the ebb. This implies that there must be a sizable change in vertical stratification in the along-channel direction, which is advected upstream during the flood and reaches the CG mooring. An along-channel survey around the time of the deployment (Fig. 10) shows that stratification is enhanced at D relative to CG. The distance between the CG and D mooring (14 km) is approximately the tidal excursion length and because vertical stratification increases seaward between

Fig. 9 Tidal phase average of the terms in equation $\partial\phi/\partial t$ (9). **a, b** “Along-tidal,” “cross-tidal,” “exchange,” and “along-adv. strat.” terms. **c, d** $\partial\phi/\partial t$, the sum of the terms on **a** and **b**, and the residual term for times of high and low stratification

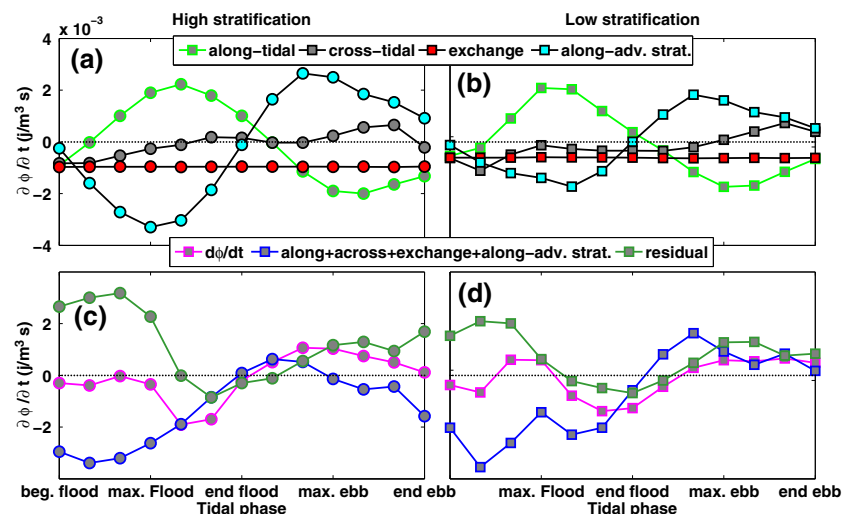
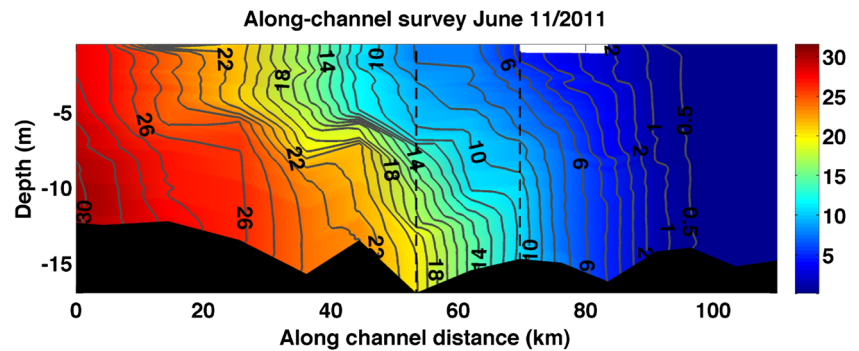


Fig. 10 Along-channel survey on June 11, 2011, showing the salinity contours in gray. The dashed vertical lines show the location of the C-line and D mooring, approximately 68 and 54 km, respectively, from the entrance of the bay. Kilometer zero is near the mouth of Delaware Bay



these moorings, it is likely that the advection of stratification is important.

The contributions from the along-channel straining and the along-channel advection of stratification are the largest but opposite in sign, and then their combined effect is not as large as the individual components but not negligible either. Their net contribution is a stratifying effect during the flood and de-stratifying effect during the ebb and is comparable with the contribution from the cross-channel flows and the exchange circulation. Consequently, the cross-channel and subtidal flows can have an important effect on stratification at tidal time scales. The combined effect of the four advective terms (blue line Fig. 9c, d) produces a stratifying effect during the flood tide, for both periods of high and low stratification.

The residual term is due to a combination of unresolved terms (mixing, vertical advection), the neglect of $\partial H/\partial t$, and estimate errors. The residual term is positive throughout the flood and most of the ebb with the highest values during flood and during times of high stratification (Fig. 9c, d). A positive residual is consistent with vertical mixing. We estimated the value of eddy diffusivity (K_s) required to generate

the observed residuals, assuming a constant eddy diffusivity and using the observed bottom to surface salinity difference. Eddy diffusivities of $2 - 4 \times 10^{-4} \text{ m}^2/\text{s}$ were required to obtain the observed residuals during times of high stratification and $5 - 8 \times 10^{-4} \text{ m}^2/\text{s}$ during times of weak stratification, with the higher values in each case occurring during the flood tide. These values of K_s fall within range of estimates by Geyer et al. (2008) and suggest that mixing is likely the dominant term associated with the residual al term. Tidal period vertical advection would cause the residual term to change signs from flood to ebb because of the reversal in the cross-channel flows. While some sign change is observed, it is not consistent with what we would expect from vertical advection, suggesting that this mechanism is not the main contributor in the residual term. The largest error is likely associated with the discretization of salinity in the vertical by the four salinity sensors. A numerical estimate of the mixing term obtained from a high-resolution profile differed by only 10 % from a four-point piecewise profile, suggesting that the residual associated with the discretization is small compared to mixing. Finally, the neglect of $\partial H/\partial t$ would produce an error of approximately 10 %.

Fig. 11 Tidal phase average of along-channel velocity (a, c) and cross-channel velocity (b, d) for times of high and low stratification. For the cross-channel velocities, positive velocities are towards the New Jersey side and negative velocities towards the Delaware side

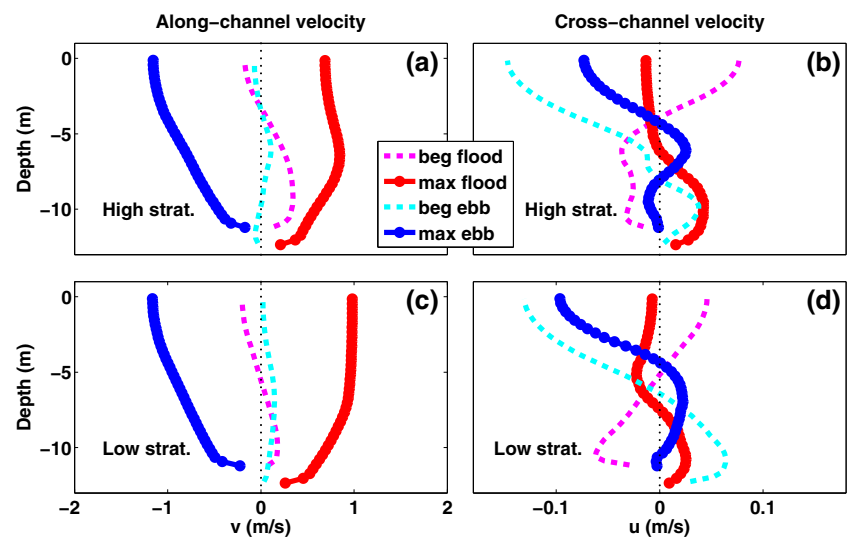
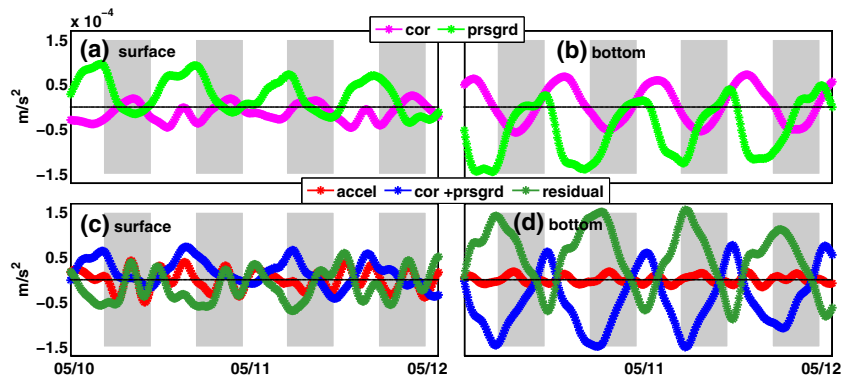


Fig. 12 Detail of the time series of the cross-channel momentum equation as expressed in Eq. 11 between March 10 and 12, 2011, for the surface (a, c) and the bottom (b, d). The shaded areas represent periods of flood tide. The residual term is equal to the acceleration term (“accel”) minus Coriolis (“cor”) minus the baroclinic pressure gradient (“prsgrd”)



In summary, the above analysis suggests that most of the observed residual is not associated with error rather with vertical mixing.

5.6 Cross-channel dynamics

The cross-channel flows have an influence on the tidal variability of stratification, and therefore we next diagnose the lateral momentum budget to understand what is driving the cross-channel flows and how they affect the density field.

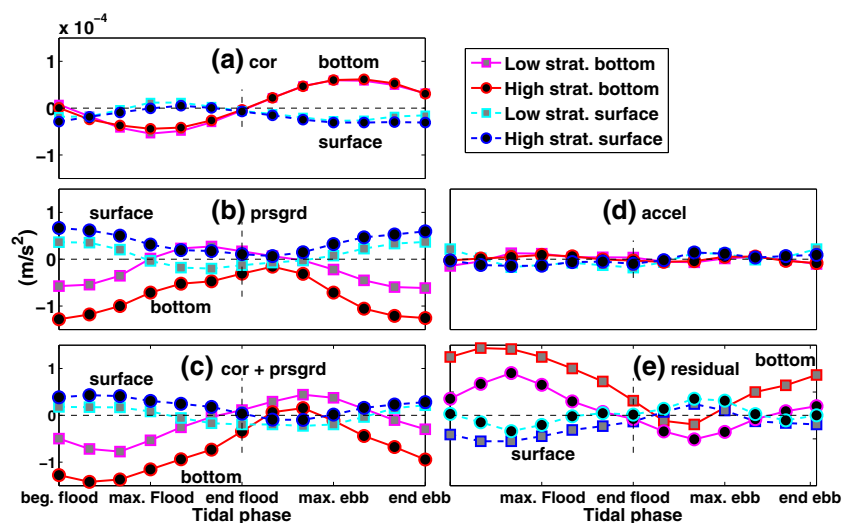
The cross-channel flows at mooring C5 (Fig. 11) consist mostly of a single circulation cell throughout most of the tidal cycle. During the beginning of flood, the circulation is clockwise (i.e., bottom flows towards Delaware), but before maximum flood, the lateral flows begin to weaken and eventually flow counterclockwise, with particularly swift surface currents flowing towards the Delaware side at the beginning of ebb. During maximum ebb, lateral flows show a hint of a three-cell system during highly stratified conditions, but remain primarily a single cell with surface flows towards Delaware and bottom/mid-water column flows towards New Jersey. Note that lateral flows for both phases of the tide

are maximum at the surface around slack water, which we interpret to be due to lateral gravitational adjustment of a cross-channel density gradient setup during the previous phase of the tide. To assess this interpretation, we then analyze the cross-channel dynamics.

Terms in Eq. 11 that describe the tendency to drive cross-channel shear are shown in Fig. 12. Near the surface, the cross-channel baroclinic term and the Coriolis are of opposite sign; however, they do not balance, as evidenced by the prominence of the acceleration term. In the lower layer, these two terms appear to be in quadrature and their amplitude is twice as large as at the surface. The acceleration term is much smaller than the Coriolis and baroclinic terms combined, and as a result, the residual term is quite significant, indicating the likely importance of the vertical stress divergence.

A tidal phase average of Coriolis and the cross-channel baroclinic pressure gradient provides insight into how these two forces drive the cross-channel circulation. The Coriolis term $f(v - \bar{v})$ (Fig. 13a), driven by the shear in the along-channel flow, is stronger during the ebb than during the flood at the surface. During the flood, vertical shear in the along-channel flow is largely confined to the bottom

Fig. 13 Tidal phase average of the different terms of the cross-channel momentum equation (Fig. 11). **a** Coriolis minus its depth average, **b** cross-channel baroclinic pressure gradient minus its depth average, **c** the sum of (a) and (b), **d** acceleration minus its depth average, and **e** the residual term, equal to the acceleration term (“accel”) minus Coriolis (“cor”) minus the baroclinic pressure gradient (“prsgrd”), for times of high and low stratification. Positive x values are towards New Jersey and negative values are towards Delaware



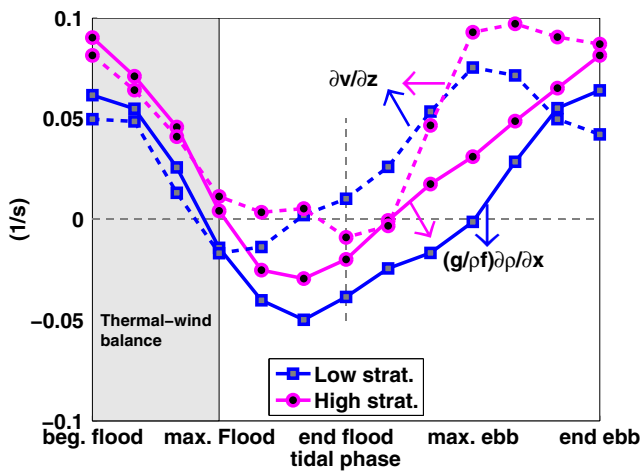


Fig. 14 Tidal phase average of $(g/\rho f)\partial\rho/\partial x$ and $\partial v/\partial z$ (at mid-depth) for times of low and high stratification. The arrows show the curves that correspond to each term

boundary layer, and thus, at the bottom, the Coriolis term is negative and accelerates the fluid towards the left (Delaware). At the surface, Coriolis weakly drives a circulation in the opposite direction except during the first 2 h of the flood tide when there is a lag between the time the surface and bottom along-channel vertical shears change sign. During the ebb, the Coriolis term drives lateral flows in the opposite direction with the lower layer accelerated towards the New Jersey shore and the upper layer towards the Delaware shore.

The magnitude of the cross-channel baroclinic term (Fig. 13b) weakens through the flood tide and gains strength through the ebb tide during high stratification conditions. During low stratification conditions, it changes sign halfway through each tidal cycle. This is consistent with a main channel that is saltier than the flanks at the beginning of the flood tide, but as the flood progresses, the main channel salinity is close to (high stratification) or fresher than (low stratification) the salinity of the flanks. During the ebb tide,

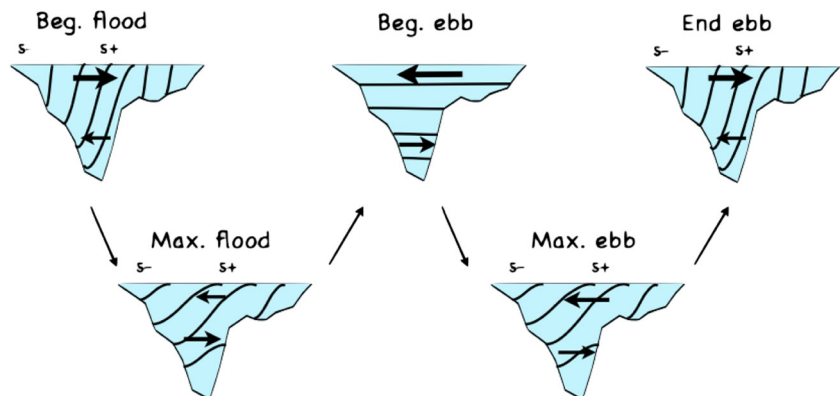
the main channel becomes progressively saltier than the flanks. Note that the sign of the cross-channel salinity gradient during the second half of the flood is inconsistent with differential advection, which would continue to increase the cross-channel salinity gradient throughout most of the flood tide.

The cross-channel circulation is consistent with the circulation driven by the combination of Coriolis and cross-channel pressure gradient (Fig. 13c). During the first half of flood, the circulation is clockwise, but during the second half, the circulation consists of a weak counterclockwise circulation. The reason for this is that the Coriolis acceleration is relatively weak at the surface because the shear in the along-channel velocity is weak in the upper 6 m of the water column (Fig. 11a, c). When this weak Coriolis force is combined with the cross-channel baroclinic pressure gradient, baroclinicity dominates over Coriolis. During the first part of ebb, the baroclinic pressure gradient is weak and Coriolis predominates over the baroclinic term (Fig. 13a, b) to produce strong near-surface cross-channel flows (counterclockwise circulation) during the early ebb. However, through the second half of the ebb, the main channel becomes increasingly saltier than the flank, and as a result, the cross-channel baroclinic term opposes Coriolis and reverses the lateral flows.

The tidal phase average of the acceleration term $\partial u/\partial t$ (Fig. 13d) shows that its magnitude is relatively small compared with Coriolis and cross-channel baroclinic pressure gradient. As a consequence, the residual term is large (Fig. 13e), in particular at depth, indicating that friction is closely balancing Coriolis and the baroclinic pressure gradient.

A tidal phase average of $\partial v/\partial z$ and $(g/\rho f)\partial\rho/\partial x$ at mid-depth shows that a thermal wind balance holds only during the first half of flood tide (Fig. 14). This implies that during this period, the cross-channel flows (at mid-depth (~ 5 m)) do not experience any acceleration, and so the cross-channel flows are either constant or zero around this depth. This is

Fig. 15 Cartoon depicting the cross-channel circulation and salinity field for different tidal phases. The oceanward direction is out of the page



shown in Fig. 11b, where around a 5-m depth, the flows are close to zero and approximately correspond to the depth where the lateral flows change sign in the surface layer.

In summary, the observed cross-channel circulation is driven by the interplay between Coriolis and the cross-channel baroclinic pressure gradient, which is itself modified by the cross-channel flows. The cross-channel flows are not purely Ekman in nature because they are strongly modified by lateral baroclinicity. The initiation of the cross-channel flows on both phases of the tide is consistent with Ekman flows, but the flow itself sets up a cross-channel pressure gradient that contributes significantly to the cross-channel momentum equation. The cross-channel circulation pattern, along with the tidal variability in the cross-channel density gradient and stratification, is depicted in Fig. 15. This shows enhanced stratification throughout the flood and weakening stratification towards the end of ebb.

6 Discussion

The tidal cycle survey (Fig. 3) illustrates how the density field changes through the tidal cycle and then produces the observed tidal variability in vertical stratification. At the end of the ebb, the isohalines are tilted, and therefore vertical stratification is reduced. There is a strong cross-channel density gradient that forces the isohalines to adjust until they become horizontal, increasing stratification, towards maximum flood. Close to maximum ebb, the isohalines remain flat, but there is a clear one cell circulation consistent with Coriolis forcing. This counterclockwise circulation strains the isohalines, and, by the end of ebb, they again have a significant slope.

This tilting/relaxation of the isohalines creates a fluctuation in the cross-channel density gradient (Fig. 6d). While we did not make an estimate of the contribution of differential advection to the cross-channel density gradient, the tendency for the salinity in the main channel to become fresher or the same salinity as the Delaware flank in the last part of the flood indicates that differential advection is not the dominant mechanism behind the tidal period variability in the cross-channel salinity gradient. Instead, it is the process of tilting of the isohalines in the cross-channel direction and the subsequent readjustment of the buoyancy that determines the tidal period variability in the cross-channel density gradient.

The traditional model of an estuary that is less stratified during the flood than during the ebb is based on the tidal straining mechanism proposed by Simpson et al. (1990). It is demonstrated that this tidal variability in stratification does not hold in a cross section in the middle reach of Delaware Bay. Our analysis showed that even though the along-channel straining mechanism is in action, the

upstream advection of a density front at mid-depth is enough to overcome the along-channel tidal straining mechanism. In addition, the tilting/relaxation of the isohalines in the cross-channel direction reinforces the stratifying tendency of the along-channel advection of stratification during the flood and the de-stratifying tendency during the ebb. The importance of the along and cross-channel advection of stratification has been also established in the Hudson River estuary (Scully and Geyer 2012).

The observed cross-channel flows have similar magnitudes during flood and ebb tides and for periods of high and low stratification (Fig. 11). This time variability also contrasts with previous observational (Chant 2002) and modeling (Lerczak and Geyer 2004) studies. However, both these previous studies occurred in much narrower systems, and thus the effects of the earth's rotation may be more prominent in the wider Delaware Bay. Moreover, numerical modeling results in Cheng et al. (2009) revealed that the inclusion of a turbulence closures scheme, in contrast to the constant eddy viscosity in Lerczak and Geyer (2004), increased the strength of lateral flows during stratified conditions.

Analysis of tidally averaged momentum equation presented by both Lerczak and Geyer (2004) and Scully et al. (2009) suggests that nonlinear advection associated with lateral circulation rectifies the estuarine exchange flow. However, the tidal rectification they describe relies on specific tidal and spring/neap variability in the lateral flows, which is not evident in this study. While it is possible that the lateral flows observed here also rectify the exchange flow, the fact that their tidal period variability differs dramatically from those studies suggests that investigation of the tidal rectification by lateral flows in wider estuaries is warranted.

Modeling results (Aristizábal and Chant 2013) revealed that secondary flows play an important role in determining the tidal period variability in salinity and driving the phase between salinity and along-channel velocity out of quadrature. When the phase between salinity and along-channel velocity are in quadrature, i.e., maximum salinity occurs at the end of flood and minimum salinity coincides with the end of ebb, the tidal motion yields no net salt flux. In this case, the time rate of change in salinity is driven solely by the along-channel advection of the along-channel salinity gradient:

$$\frac{\partial s_t}{\partial t} = -v_t \frac{\partial s_t}{\partial y} \quad (12)$$

where s_t and v_t are the tidally varying salinity and tidally varying along-channel velocity. However, as other terms in the salt budget equation become important, such as the lateral advection of salt and mixing processes, s_t and v_t become out of quadrature and a net salt flux at tidal

time scales (tidal oscillatory salt flux) occurs. In addition, the modeling results indicate that the tidal oscillatory salt flux (TOSF) increases with increasing stratification. TOSF is proportional to stratification because as stratification increases, lateral circulation produces larger tidal period variability in s_t , and thus the tidal cycle average of the product of $u_t s_t$ is larger. Stratification increases with decreasing tidal current speed and thus TOSF is largest during neap tide and weakest during spring tide in contrast to existing parameterizations, which suggest that it increases with increasing tidal current speed (Banas et al. 2004 and MacCready 2007). This discrepancy is probably due to the large spring-neap variation in stratification that occurs in Delaware Bay.

7 Conclusions

Stratification in the middle reach of Delaware Bay is characterized by a reduction of the bottom to surface salinity difference during ebb tide and an increase during the flood tide for periods of high stratification. This tidal variability in stratification is contrary to the tidal variability predicted by the tidal straining mechanism introduced by Simpson et al. (1990).

We calculated the time rate of change of the potential energy anomaly as a way to quantify the different mechanisms that control vertical stratification at tidal time scales. The along-channel straining and the along-channel advection of vertical stratification are the largest contributors, but because they compete with each other, their net effect is reduced and is comparable to the cross-channel straining and the subtidal flow contributions. The net effect of the along-channel straining plus the along-channel advection of vertical stratification is enhanced stratification during flood, due to the upstream advection of a mid-depth salinity front, and reduced stratification during ebb. This tendency reinforces the action of the cross-channel flows on the density field: the tilting of the isohalines during the ebb weakens vertical stratification and the subsequent relaxation during the flood promotes water stability.

The cross-channel dynamics show that the lateral flows are driven by the combination of Coriolis and cross-channel pressure gradient. During the first half of the flood tide, the cross-channel pressure gradient and Coriolis act mostly in concert, creating a clockwise circulation that only persists during the first half of the flood tide. The circulation reverses around maximum flood and remains a counterclockwise cell for the rest of the ebb tide. During the early ebb, the cross-channel pressure gradient is weak and therefore Coriolis dominates the cross-channel pressure gradient. As the ebb progresses, the cross-channel baroclinic term opposes Coriolis and reverses the lateral flows.

Acknowledgments We thank Eli Hunter, Chip Haldeman, Joe Jurisa, Dove Guo, and the captain of the ship Ken Roma for all their dedication in collecting the data. This work was supported by a National Science Foundation grant OCE-0928567 and OCE-0825833. The author María Aristizábal was supported by a Dupont fellowship and the Institute of Marine and Coastal Sciences at Rutgers University. We also thank Jack McSweeney for closely reading the manuscript. We are also very thankful to the reviewers who insisted in the importance of the along-channel advection of stratification.

References

- Aristizábal M, Chant R (2013) A numerical study of salt fluxes in Delaware Bay estuary. *J Phys Oceanogr* 43(8):1572–1588
- Banas NS, Hickey BM, MacCready P (2004) Dynamics of Willapa Bay, Washington: a highly unsteady, partially mixed estuary. *J Phys Oceanogr* 34:2413–2427
- Beardsley RC, Boicourt WC (1981) On estuarine and continental shelf circulation in the Middle Atlantic Bight. MIT Press, Cambridge
- Burchard H, Hofmeister R (2008) A dynamic equation for the potential energy anomaly for analyzing mixing and stratification in estuaries and coastal seas. *Estuar Coast Shelf Sci* 77:679–687
- Chant RJ (2002) Secondary circulation in a region of flow curvature: relationship with tidal forcing and river discharge. *J Geophys Res* 107(C9):14–1–14–11
- Chant RJ, Stoner AW (2001) Particle trapping in a stratified flood-dominated estuary. *J Marine Res* 59:29–51
- Cheng P, Wilson RE, Chant RJ, Fugate DC, Flood RG (2009) Modeling influence of stratification on lateral circulation in a stratified estuary. *J Phys Oceanogr* 39:2324–2337
- de Boer GJ, Pietrzak JD, Winterwerp JC (2008) Using the potential energy anomaly equation to investigate tidal straining and advection of stratification in a region of freshwater influence. *Ocean Model* 22:1–11
- Garvine RW, McCarthy RK, Wong KC (1992) The axial salinity distribution in the Delaware estuary and its weak response to river discharge. *Estuar Coast Shelf Sci* 35:157–165
- Geyer WR, Chant R, Houghton R Tidal and spring-neap variations in horizontal dispersion in a partially mixed estuary. *J Geophys Res* C 2008. doi:10.1029/2007JC004644
- Jay DA, Smith JD (1990) Circulation, density distribution and neap-spring transitions in the Columbia River estuary. *Prog Oceanogr* 25(14):81–112
- Lacy J, Stacey MT, Burau JR, Monismith SG (2003) Interaction of lateral baroclinic forcing and turbulence in an estuary. *J Geophys Res* 108(C3):34,1–34,15
- Lerczak JA, Geyer WR (2004) Modeling the lateral circulation in straight, stratified estuaries. *J Phys Oceanogr* 34:1410
- Li Y, Li M (2012) Wind-driven lateral circulation in a stratified estuary and its effects on the along-channel flow. *J Geophys Res* 117(C9):C09005
- MacCready P (2007) Estuarine adjustment. *J Phys Oceanogr* 37:2133–2145
- MacCready P (2011) Calculating estuarine exchange flow using isohaline coordinates. *J Phys Oceanogr* 41:1116–1124
- Nepf HM, Geyer WR (1996) Intratidal variations in stratification and mixing in the Hudson estuary. *J Geophys Res* 101(C5):12,079–12,086
- Rippeth TP, Fisher NR, Simpson JH (2001) The cycle of turbulent dissipation in the presence of tidal straining. *J Phys Oceanogr* 31:2458–2471

- Scully ME, Geyer WR (2012) The role of advection, straining, and mixing on the tidal variability of estuarine stratification. *J Phys Oceanogr* 42:855–868
- Scully ME, Geyer WR, Lerczak JA (2009) The influence of lateral advection on the residual estuarine circulation: a numerical modeling study of the Hudson River estuary. *J Phys Oceanogr* 39(1):107–124
- Sharples J, Simpson J (1995) Semi-diurnal and longer period stability cycles in the Liverpool Bay region of freshwater influence. *Cont Shelf Res* 15(2/3):295–313
- Sharples J, Simpson JH, Brubaker JM (1994) Observations and modelling of periodic stratification in the Upper York River estuary, Virginia. *Estuar Coast Shelf Sci* 38(3):301–312
- Simpson J (1981) The shelf-sea fronts: implications of their existence and behaviour. *Philos T R Soc Lond Series A* 302:531–546
- Simpson J, Bowers D (1981) Models of stratification and frontal movement in shelf seas. *Deep-Sea Res* 28(7):727–738
- Simpson J, Hunter J (1974) Fronts in the Irish Sea. *Nature* 250:404–406. (August)
- Simpson J, Hunter J (1978) Fronts on the continental shelf. *J Geophys Res* 83(C9):4607–4614
- Simpson J, Brown J, Matthews J, Allen G (1990) Tidal straining, density currents and stirring in the control of estuarine stratification. *Estuaries* 13(2):125–132
- Simpson JH, Souza AJ (1995) Semidiurnal switching of stratification in the region of freshwater influence of the Rhine. *J Geophys Res* 100(C4):7037–7044
- Souza A, Simpson J (1996) The modification of tidal ellipses by stratification in the Rhine ROFI. *Cont Shelf Res* 16(8):997–1007
- Souza AJ, Simpson JH (1995) A two-dimensional (x-z) model of tidal straining in the Rhine ROFI. *Cont Shelf Res* 16(7):949–966
- Stacey MT, Monismith SG, Burau JR (1999) Observations of turbulence in a partially stratified estuary. *J Phys Oceanogr* 29(8):1950–1970
- USGS (2012) Delaware River at Trenton NJ
- Wong KW (1994) On the nature of transverse variability in a coastal plain estuary. *J Geophys Res* 99:14,209–14,222